The Sea-Breeze-Induced Coastal Calm Zone as Revealed by Satellite Data and Simulated by a Numerical Model

ROBERT W. FETT AND PAUL M. TAG

Naval Environmental Prediction Research Facility, Monterey, CA 93943

(Manuscript received 17 January 1984, in final form 27 March 1984)

ABSTRACT

Meteorological satellite scanning radiometer data from a visual sensor during daylight hours are characteristically influenced by sunglint from the ocean surface as the sensor scans in the direction toward the sun (between the satellite subpoint and solar subpoint). When seas are calm in the region near the primary specular point (PSP), the sun's rays are either reflected directly into the spacecraft sensor yielding a high energy (bright) response, or away from the sensor yielding a low energy (dark) response. The particular effect depends on the proximity of the calm area to the PSP. This paper shows examples of bright and dark linear patterns adjacent to and tending to parallel coastlines. The patterns are interpreted to be sea-breeze-induced calm zones originating during periods of offshore flow when the pressure gradient causing the sea breeze is exactly counterbalanced by the larger-scale synoptic gradient. A two-dimensional planetary boundary layer (PBL) numerical model successfully simulates this condition and additionally shows that the calm region first appears near the coastline as daytime heating commences and then moves seaward with time as afternoon heating over land is maximized. We show that, at least initially, the rapidity of movement and the distance covered in this movement are directly related to the land–sea temperature contrast and indirectly related to the speed of the offshore flow, and are highly sensitive to small changes in these parameters.

1. Introduction

Satellite visible images of coastal areas under conditions of sunglint often reveal especially bright or especially dark offshore linear patterns. These patterns tend to parallel sections of the coastline at varying distances from the coast, up to 150 km. The patterns can be interpreted as an effect of calm or near-calm sea state where the sun's rays are either reflected directly to the spacecraft sensor (producing a bright tone) or away from the spacecraft sensor (producing a dark tone). The geometrical aspects leading to this effect change continually for polar-orbiting satellites, depending on the location of the area with respect to the satellite and the instantaneous position of the subpolar point of the sun in its seasonal and daily cycle. Further details concerning this use of sunglint interpretation have been described and illustrated in a number of examples (Parmenter, 1969; McClain and Strong, 1969; Fett and Mitchell, 1977).

Previously, such sunglint effects were shown to exist primarily along the axes of ridge lines over marine areas, extending from centers of high pressure (Anderson *et al.*, 1974). More recent research at the Naval Environmental Prediction Research Facility (NEPRF) has revealed numerous examples of these phenomena along the axes of near-equatorial troughs which, similar to ridge lines, are also characterized by wind speed minima.

On a mesoscale basis, bright and dark patterns frequently denote the protected calm lee regions of island barriers (Strong *et al.*, 1974; Fett and Rabe, 1976; Fett and Burk, 1981). The edges of oceanographic features also are often revealed in sunglint through light and dark reflective effects, cold water tending to be calmer than warm water. Because of this characteristic, visible satellite imagery over sunglint regions often reveals oceanographic details as well as, or better than, the corresponding infrared data.

Finally, such effects have at times been noted in conjunction with convective cloud line development over marine areas, the dynamics of the cloud line circulation apparently having an influence on the state of the sea in the region adjoining the cloud line development.

A most likely cause for a calm sea zone adjacent to a coastal area during daylight hours is the sea-breeze circulation at low levels where it is counterbalanced by the offshore flow.

In this paper, examples of such effects are shown with available documentation. A two-dimensional planetary boundary-layer (PBL) model, applied to the task of analyzing sea-breeze effects as the day progresses from morning through noon to the afternoon, successfully simulates the sea-breeze circulation and provides additional diagnostic detail.

It is shown that when the basic synoptic flow is offshore, a zone of minimum wind speed first appears

near the coast as daytime heating of the land commences. The calm area moves seaward with time into the late afternoon when it may be found 150 km or more offshore, depending on the speed of the basic synoptic flow and the thermal contrast between the land and sea. Under synoptic conditions of onshore flow the sea breeze merely accelerates the basic synoptic flow, and the calm strip does not appear.

2. Satellite examples

a. Case 1

Figure 1 is a Gemini XII manned-spacecraft photograph of the southern tip of Florida at 1413 Eastern Standard Time (EST) 12 November 1966. Sunglint is apparent in the surrounding waters, becoming brightest in the region off the west coast in the Gulf of Mexico. In this region a dark strip indicating calm seas can be seen approximately 45 km offshore, paralleling the coast.

Low-level flow from the east can be deduced from the suppressive effect of Lake Okeechobee which inhibits cloud formation to the west because of its cooling effect on air that has passed over its boundary. Note also the enhanced sea breeze cloud line that has formed inland of the east coast, while no such effect appears along the west coast. Such convection would be expected to extend farther inland where the sea-breeze effect was adding to the strength of the basic synoptic flow, rather than countering it as on the west coast. Hourly weather observations for Sarasota on the northern portion of the west coast indicated offshore easterly flow until 1100 EST when the sea breeze was initiated from the west with a speed of 2.5 m s^{-1}. This flow increased in speed to 5 m s^{-1} at the time of the Gemini photograph.

Figure 2 is the National Meteorological Center's (NMC) surface analysis over the area for this date at 0700 EST (henceforth all times are EST). The analysis shows light easterly offshore flow in the region from Tampa southward to Key West.

b. Case 2

In another sunglint example in a Defense Meteorological Satellite Program (DMSP) image (Fig. 3; 1107 3 June 1979), this time with low-level flow from the west, the dark strip appears off the opposite coast of

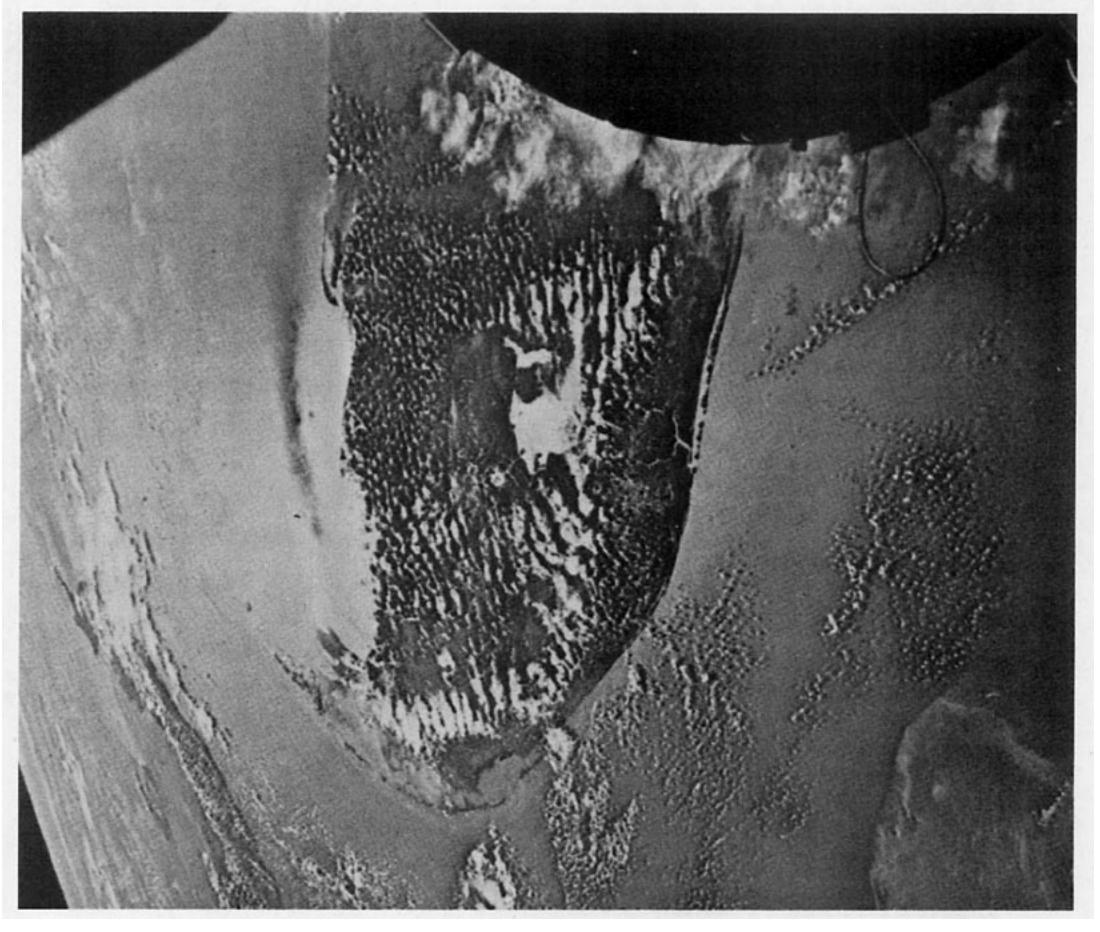

FIG. 1. A Gemini XII manned spacecraft photograph of the southern tip of Florida at 1413 EST 12 November 1966. The dark strip off the west coast is a sunglint effect implying calm seas (Case 1).

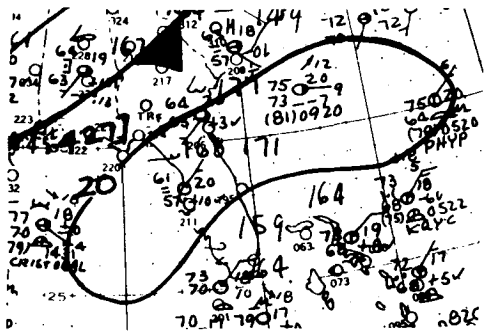

FIG. 2. The wind flow field near the time of Fig. 1, as depicted by the NMC surface analysis for 0700 EST 12 November 1966. Wind arrows with no barbs indicate speeds of less than 2.5 m s^{-1}; short barbs represent wind speed increments of 2.5 m s^{-1}, and long barbs, increments of 5.0 m s^{-1}.

Florida. Again, the suppressive effect of Lake Okeechobee on convective cloud formation, this time to the east, verifies the westerly low-level winds. Smaller lakes to the north also exhibit a cloudiness minimum on their east sides, implying westerly flow. The NMC surface analysis for this date (Fig. 4) at 0700 shows that flow was light but it did have a westerly component along the east coast as suggested by the satellite data.

The time of the satellite image in this case was about three hours earlier than the previous example. It is of special interest, therefore, to note that the calm region here is much closer to shore at a distance of approximately 20 km, as opposed to about 45 km for the previous example. It will be shown numerically that these calm regions move seaward as the day progresses and that their location and speed of movement are a function of the speed of the basic synoptic flow and the land–sea temperature contrast.

c. *Case 3*

A final example of the effect appears in DMSP visible imagery over the region near Florida at 1223 6 June 1973 (Fig. 5). In this particular example, gray shade

FIG. 3. DMSP visual (0.54 km resolution) enlargement of the Florida region at 1107 EST 3 June 1979. The dark strip offshore of the east coast is a sunglint effect implying calm seas (Case 2).

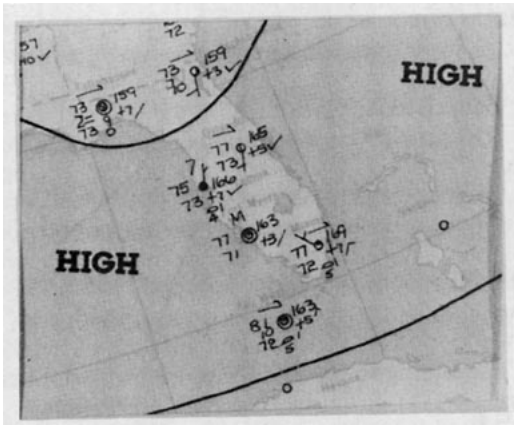

FIG. 4. The wind flow field near the time of Fig. 3, as depicted by the NMC surface analysis for 0700 EST 3 June 1979.

tonality is reversed from dark to bright; because of the changed geometric perspective placing the coastline area near the center of a sunglint pattern, the sun's rays over calm regions are reflected directly into the spacecraft sensor rather than away from it. The effect is seen to occur near the shoreline of the west coast of Florida and is particularly pronounced near Marco Island, just north of the southern tip of the peninsula. Surface flow was stronger on this date than in the other two examples. The NMC surface analysis for 0700 (Fig. 6) shows 5 m s^{-1} winds from an easterly direction at Tampa, Miami and Key West. Cloud streets over Florida show an east–west orientation, while the suppression of convective cloudiness downstream (to the west) of Lake Okeechobee and other smaller lakes verifies the easterly low-level wind direction.

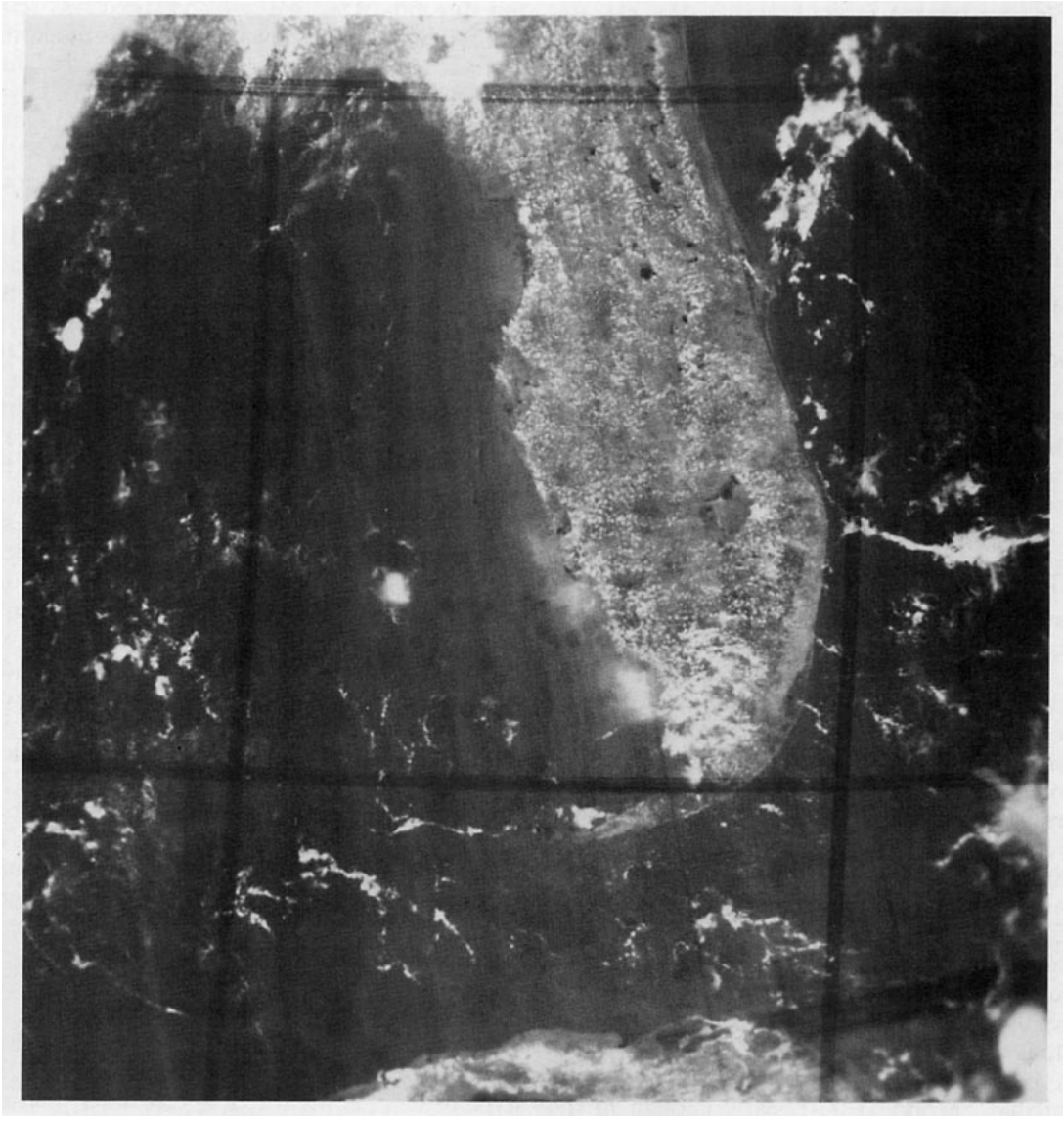

FIG. 5. DMSP visual (0.54 km resolution) enlargement of the Florida region at 1223 EST 6 June 1973. Calm seas are implied by brilliant sunglint reflection along the southwest coast.

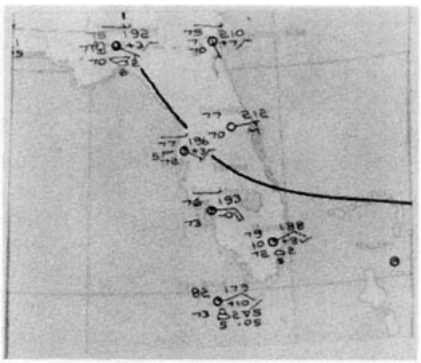

FIG. 6. The wind flow field near the time of Fig. 5, as depicted by the NMC surface analysis for 0700 EST 6 June 1973.

The fact that the reflective calm sea pattern is so close to shore in this example appears to be directly related to the strength of the offshore flow. From a qualitative point of view this appears reasonable since a stronger low-level synoptic flow would require a correspondingly stronger sea-breeze counter flow to produce a net calm condition. This would logically tend to occur later in the day near the shore.

3. Numerical simulations

To explore the development of a calm region at sea during a sea-breeze period, we made use of the NEPRF two-dimensional planetary boundary-layer model. This model was developed to explore PBL changes both over open ocean and over land–ocean interfaces. Basically, the model is a set of partial differential equations solved on a staggered (Arakawa Scheme C) grid (Tag and Rosmond, 1980). Predicted variables are u, v, w, θ and r (east–west, north–south and vertical wind components, potential temperature and mixing ratio). The important processes with respect to maritime simulations are advection, turbulent mixing and radiation. However, because we were interested only in the dynamics of the simulations, and because clouds are not an important feature of the simulations, we turned off both short- and longwave radiation. The vertical turbulent mixing of momentum, heat and moisture is based on K-theory (Tag, 1983) and the Businger surface flux formulations (Businger *et al.*, 1971) as configured by Barker and Baxter (1975).

Our intended goal was to predict the calm wind areas implied in Figs. 1, 3 and 5 (hereafter representing Cases 1, 2 and 3). Because the observed minima were fairly uniform along sections of the Florida coast (more so in Cases 1 and 2), a reasonable simplification was to model the situation in two dimensions only.

All three situations were initialized at 0700. This time was convenient for two reasons. First, a sounding was available. Second, 0700 is early enough in the morning that the surface and air (near-surface) temperatures can be assumed to be nearly equal. Cases 1, 2 and 3 were initialized, respectively, with the 0700 soundings for Key West, Florida (12 November 1966), West Palm Beach, Florida (3 June 1979) and Miami, Florida (6 June 1973). We assumed that this initializing sounding was valid over both the 0700 land and ocean areas. While this assumption is obviously not correct, the period shortly after sunrise is the one period during a 24-hour day when land–sea vertical temperature profile differences should be minimal.

The initializing wind profile, on the other hand, was the most important factor in our simulations here. The Case 1 sounding revealed a wind uniform with height (through 4 km), from the east at about 1.5 m s^{-1}. For Case 2 the observed sounding revealed no measured wind throughout the PBL at 0700. However, other observations as well as Fig. 3 (discussed earlier) indicated a light west-southwesterly flow. Accordingly, this direction was used and the speed was set to 1.5 m s^{-1}. The observed flow in Case 3 was much stronger and was variable with height. The initial wind direction was set at east-northeasterly, with a surface flow of 5.1 m s^{-1} and the upper-level flow at 2 m s^{-1}. Note that the flow directions specified in Cases 2 and 3 were actually perpendicular to the coastline; the flow in Case 1 was nearly so.

Nearly as important as the initializing wind profile is the land–sea temperature contrast. This temperature difference provides the driving force behind the sea-breeze circulation. Because Case 1 occurred during November and Cases 2 and 3 in June, the land–sea temperature contrasts cannot be expected to be the same for these two months. One steady (nondiurnally-varying) point for the temperature difference is the climatic ocean temperatures off the west and the east coasts of Florida. The monthly climatic summaries of Meserve (1974) provide November and June sea-surface temperatures of 26 and 28°C. (It so happens that both the Gulf and Atlantic June temperatures are 28°C.) While these water temperatures can be regarded as reasonably constant during a diurnal cycle, the surface temperatures over land can vary considerably, particularly during the daytime.

To assist in determining the land–sea temperature contrasts, use was made of infrared satellite data. Surface temperatures across various sections of Florida and the offshore water region were determined using an algorithm which computes temperature as a function of gray-shade value. Although the algorithm did not correct for errors due to water vapor absorption (implying that the absolute temperature may not be accurate), the main interest in temperature gradients makes this limitation less important.

Our data base was the GOES-East satellite data for 1982. Because the land-surface temperature is related primarily to the time of day, the time of year, and the type of surface, the use of a year other than those in our experiments was not considered detrimental to

our purpose. Several cloud-free times in May (June was unavailable) and November provided representative land–sea contrasts; these were generally between 1100 and 1330, a desirable period for our purposes. (Note that Cases 2 and 3 were in early June.) Analysis of these data yielded a 6.0 and 8.5°C land–sea difference at solar noon for November and May, respectively. These data, together with the November and June climatological sea-surface temperatures above, were integrated to define the land-surface temperature variation used in the three cases (see Fig. 7).

Further details regarding the model simulations are as follows. All three cases were run from 0700 to 1700 with a two-dimensional domain having 20 horizontal and 16 vertical grid points. Of the 20 horizontal grid points, one-half were assumed to represent land and the other one-half water. All cases were run initially with a 15 km grid spacing. In order to provide additional resolution, Cases 2 and 3 were rerun with finer resolution (see next section). The top of the domain was set at 5 km, with a stretched grid maximizing resolution near the ground. The lowest grid point above the surface was at 10 m, the height for which the total wind speed will be illustrated shortly. The roughness speed length for land was set at 0.04 m and for water at 0.0001 m.

4. Model results

The model output that is of interest is the surface wind speed and its variation with distance from the coastline. The qualitative arguments presented earlier to explain the sunglint effects (Figs. 1, 3 and 5) suggest that a minimum in the surface wind speed should be predicted at the appropriate distance from shore. In terms of the model output, the first grid point (10 m) above the surface is the one of interest.

We consider Case 1 (Fig. 1) first. This west coast situation (November) revealed a dark band parallel to the coast-line at distances from 30 to 60 km offshore. As described before, the pertinent conditions for this experiment are: 1) an initial easterly wind of 1.5 m s^{-1}, uniform with height; 2) an offshore Gulf water temperature of 26°C; and 3) the mean November land temperature variation of Fig. 7.

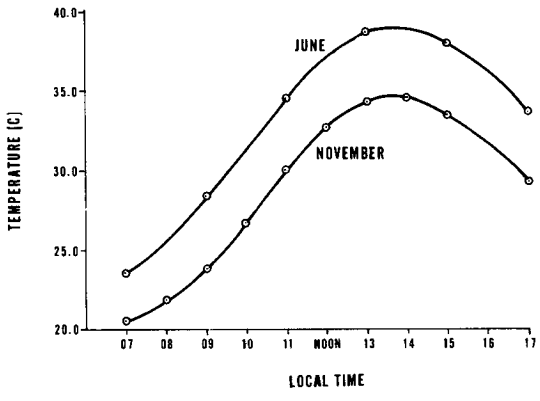

FIG. 7. Surface temperature variation over land in Florida.

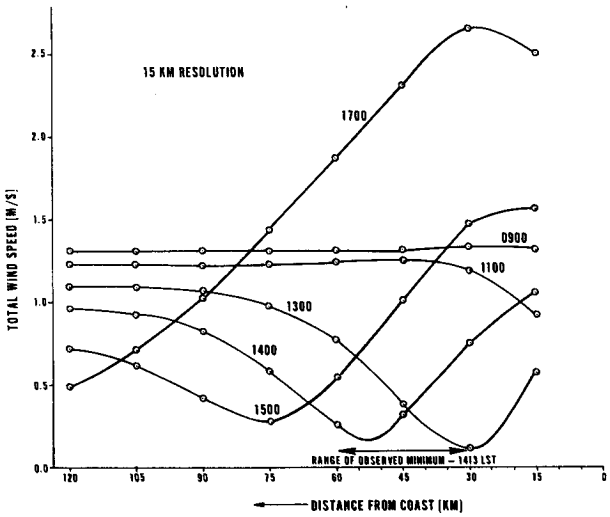

FIG. 8. Model-predicted 10 m wind speed as a function of distance from coast for the situation depicted in Fig. 1 (Case 1). Numbers associated with each curve represent local standard time (LST).

We plotted the total wind speed as a function of distance from the coastline for several times during the 10 h simulation (Fig. 8). Starting at 0900, note that the wind speed is nearly constant from the shoreline outward. Two hours later, at 1100, the sea breeze first becomes evident by a reduction in the wind speed near the shore. By 1300, a decided minimum in the wind distribution is evident at 30 km. By 1500 the minimum has moved to 75 km offshore, and by 1700 the minimum has moved beyond 120 km. Because the spacecraft photograph was taken at 1413, the 1400 time plot was added. A linear interpolation between 1400 and 1500 places the computed minimum at slightly less than 60 km at 1413. This location is just within the range of the observed minimum.

In contrast to Case 1, Case 2 represents an east Florida situation during the month of June. Again, a black band parallels the coast (Fig. 3), from approximately 10 to 30 km offshore. The pertinent conditions for Case 2 are: 1) an initial west-southwesterly 1.5 m s^{-1} flow, uniform with height; 2) an offshore Atlantic Ocean temperature of 28°C; and 3) the June land temperature variation of Fig. 7. In contrast to the 1413 observation time in Case 1, the satellite photograph in Fig. 3 was acquired three hours earlier at 1107.

The format for the wind variation plot for this case (Fig. 9) is identical to that of Fig. 8 except that the shoreline is now to the left. Again, the wind speed was plotted every two hours from 0900 to 1700 and, as in Fig. 8, the wind speed minimum moves seaward from the shoreline as the day progresses. The striking difference between Cases 1 and 2 lies in the speed with

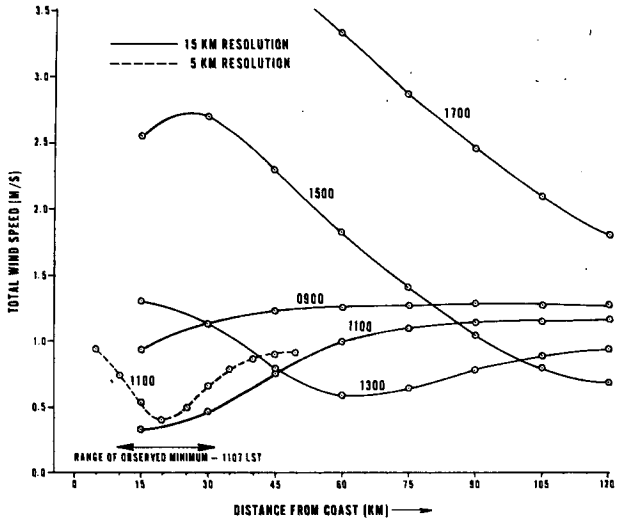

FIG. 9. As in Fig. 8 but for situation depicted in Fig. 3 (Case 2).

which this minimum moves, roughly twice as fast in Case 2 (e.g., the minimum at 1300 is located at 30 km in Fig. 8 and 60 km in Fig. 9). Because the initial offshore wind flow is nearly identical for the two cases, the difference must lie in the 2.5°C larger (at solar noon) land–sea surface temperature difference for the June simulation. Of course, the concern here is the location of the model-calculated minimum at the observation time of 1107. The initial model simulation which used a horizontal grid spacing of 15 km (solid lines in Fig. 9) indicates that the calculated minimum is near the observed minimum (approximately 10–30 km). To discern more accurately the exact location of the model minimum, the simulation was rerun with 5 km resolution. The dashed curve for 1100 represents this rerun. The resultant minimum now falls in the center of the range of the observed minimum.

Case 3 differs from our other two examples in that the mean offshore surface flow is much stronger (5.1 versus 1.5 m s^{-1}). The upper level flow is weaker, but it is the low-level wind that is of interest here. Like Case 1, Case 3 is a west Florida situation; but, like Case 2, use is made of the June land temperature curve (Fig. 7). Based on our above analysis of Case 2 (which uses the same June land–sea temperature variation), the more than factor of 3 wind increase here suggests that a wind speed minimum would remain close to shore for a longer period. In fact, a look at Fig. 5 (valid at 1223) shows that the highly reflective area lies directly on the shore and extends outward to ~25 km. In the lighter-wind case of Fig. 9, the minimum had moved close to 60 km at the same time. The numerical results for Case 3 are shown in Fig. 10. They confirm the qualitative analysis; the minimum still lies at the first grid point from shore as late as 1300. A rerun of the same experiment using a resolution six times greater (dashed curve) places the minimum approximately 5 km from shore at noon, well within the observed range of the minimum.

5. Discussion and summary

Satellite visible data which suggest a calm or near-calm region near a coastline have been interpreted numerically using a two-dimensional planetary boundary-layer model. The calm region appears to be that zone where the mesoscale pressure gradient causing the sea breeze is counterbalanced by the large-scale pressure gradient (during periods of large-scale offshore flow). Numerical simulations of the three case studies reveal that this calm region appears first near the coastline and then moves seaward with time as afternoon heating over the land is maximized. At least initially, the rapidity of movement and the distance covered in this movement is directly related to the land/sea temperature contrast and indirectly related to the speed of the offshore flow. In two cases which were nearly matched with regard to the speed of the offshore flow, an additional 2.5°C temperature difference between land and water caused the wind minimum to move seaward twice as fast. Comparatively, in two cases matched for land–sea temperature contrast, a synoptic surface flow of 5.1 m s^{-1} (versus 1.5 m s^{-1}) caused the wind minimum to remain near the shore for an additional two hours. It is interesting to note that, as the offshore flow becomes stronger, the percentage reduction in wind speed at the shoreline becomes less, eventually producing a negligible reduction. This effect is evident in comparing Fig. 10 to Fig. 9 (using 15 km resolution).

From a satellite-based analysis and forecast point of view, knowledge of these effects can provide a new tool for assistance in determining the direction of lower-level flow in coastal areas and the likely impact of the sea-breeze regime on sea state (and variations in sea state with time) over the same region. The calm effect

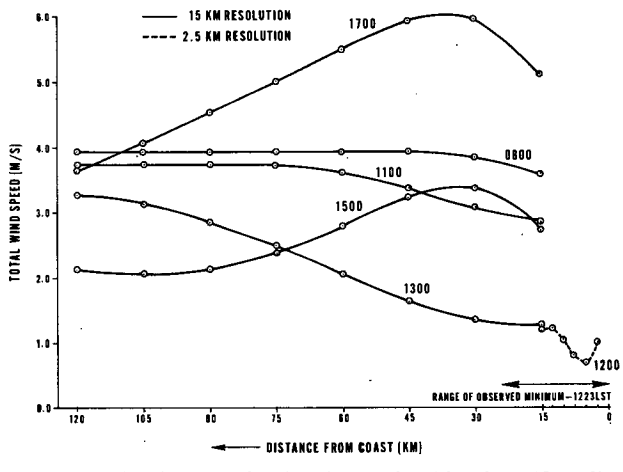

FIG. 10. As in Fig. 8 but for situation depicted in Fig. 5 (Case 3).

appears to delineate the outer limit of the counterbalanced pressure gradient at any given time; therefore, variations from day-to-day at the same time may provide clues to important changes in basic atmospheric conditions at low levels over the region. Ultimately, this may lead to a quantitative method of utilizing such information in analyzing and predicting sea-breeze strength.

Acknowledgments. The authors wish to thank Ms. Linda Rodriguez for help in locating, retrieving and processing the GOES-East infrared satellite data. The authors also acknowledge several helpful conversations with Mr. L. Robin Brody and Dr. Steven D. Burk of our facility.

REFERENCES

Anderson, R. K., and Collaborators, 1974: Application of meteorological satellite data in analysis and forecasting. ESSA Tech. Rep. NESC51, NOAA/NESS, Satellite Applications Dept., World Weather Bldg., Washington, DC 20233, 312 pp.

Barker, E. H., and T. L. Baxter, 1975: A note on the computation of atmospheric surface layer fluxes for use in numerical modeling. *J. Appl. Meteor.*, **14,** 620–622.

Businger, J. A., J. C. Wyngaard, Y. Izumi and E. F. Bradley, 1971: Flux-profile relationships in the atmospheric surface layer. *J. Atmos. Sci.*, **28,** 181–189.

Fett, R. W., and K. M. Rabe, 1976: Island barrier effects on sea state as revealed by a numerical wave model and DMSP satellite data. *J. Phys. Oceanogr.*, **6,** 324–334.

——, and W. F. Mitchell, 1977: Navy tactical applications guide, Vol. 1. Techniques and applications of image analysis. Applications Rep. 77-03, Naval Environmental Prediction Research Facility, Monterey, CA 93943, 176 pp.

——, and S. D. Burk, 1981: Island barrier effects as observed by satellite and simulated by a numerical model. *Mon. Wea. Rev.*, **109,** 1527–1541.

McClain, P. E., and A. E. Strong, 1969: On anomalous dark patches in satellite-viewed sunglint areas. *Mon. Wea. Rev.*, **97,** 875–884.

Meserve, J. M., 1974: *U.S. Navy Marine Climatic Atlas of the World,* Vol. 1: *North Atlantic Ocean.* U.S. Govt. Printing Off., Washington, DC 20402, 271 pp.

Parmenter, F. C., 1969: Sunglint. Picture of the month. *Mon. Wea. Rev.*, **97,** 155–156.

Strong, A. E., R. J. DeRycke and H. G. Stumpf, 1974: Extensive areas of reduced waves leeward of the Lesser Antilles. *J. Geophys. Res.*, **79,** 44–49.

Tag, P. M., 1983: Marine fog/stratus forecasting with a 3-D boundary layer model. *Preprints, Sixth Conf. on Numerical Weather Prediction,* Omaha, Amer. Meteor. Soc., 74–76.

——, and T. E. Rosmond, 1980: Accuracy and energy conservation in a three-dimensional anelastic model. *J. Atmos. Sci.*, **37,** 2150–2168.